Modeling the impacts of climate trends and lake formation on the retreat of a tropical Andean glacier (1962-2020)

Tal Y. Shutkin[1,2], Bryan G. Mark[1,2], Nathan D. Stansell[3], Rolando Cruz Encarnación[4], Henry H. Brecher[2*],

Zhengyu Liu[1,2], Bidhyananda Yadav[2], Forrest S. Schoessow[1]

[1]Department of Geography, The Ohio State University, Columbus, Ohio, 43210, USA
[2]Byrd Polar and Climate Research Center, The Ohio State University, Columbus, Ohio, 43210, USA
[3]Department of Earth, Atmosphere, and Environment, Northern Illinois University, DeKalb, Illinois, 60115, USA
[4]Autoridad Nacional del Agua, Huaraz, 02002, Perú
[*]Deceased

Correspondence to: Tal Y. Shutkin (shutkin.3@osu.edu)

Abstract

Located in Peru's Cordillera Blanca, the Queshque Glacier (~9.8˚S) has experienced nearly continuous retreat since the mid-20th century. More recently, this trend has accelerated after the glacier transitioned from land to lake terminating. We use observations of glacier surface height change (1962-2008), bed topography, and climatology to evaluate the relative drivers of Queshque's evolution from 1962-2020. Six Open Global Glacier Model ensemble members differing in climatic sensitivity are calibrated to fit the mass balance rate of -442 mm w.e. a[-1] calculated over the 2008 glacier area between 1962-2008. The models are then used to simulate monthly glacier mass balance over the entire study period and dynamic glacier evolution from 2008 to 2020. The models reproduce a typical outer-tropical glacier mass balance regime, showing continuous ablation throughout the year that increases during the pronounced wet season. Climatological trend analyses along with coupled mass balance and ice flow simulations indicate that temperature has been the predominant driver of mass loss since 2008 and that recent precipitation levels have caused minor dampening of this trend. The strongest negative correlation between temperature and mass balance occurs during the wet season, while a positive correlation between precipitation and annual mass balance is most pronounced during the dry season. The influence of ENSO over mass balance trends appears to decline throughout the study period except during the wettest months, suggesting that wet season Pacific sea-surface temperatures are strong predictors of outer-tropical glacier mass balance variability. Finally, frontal ablation into the newly formed lake began in 2010. This caused ice acceleration at the glacier front, an average mass loss increase of 4%, and a significant narrowing of the model ensemble mass loss spread. We conclude that while Queshque's trajectory remained coupled to climatic forcings, the new proglacial lake exacerbated and modified the retreat pattern regardless of the model climate sensitivity.

1 Introduction

Glacier-climate interactions in the tropics (23.5˚S-23.5˚N) have broad relevance across multiple timescales and applications (Mark, 2008). While tropical glaciers have varied considerably in size and extent during the Holocene (Stansell et al., 2023), they have retreated through most of the 20th and 21st centuries (Thompson et al., 2011; Vuille, 2018). Processes associated with these oscillations are of particular relevance in the Peruvian Andes, which host the majority of extant tropical ice (RGI Consortium, 2017). The present article focuses on a glacier in Peru's Cordillera Blanca (CB), a mountain range that has been reworked by multiple phases of glaciation (Mark et al., 2024) but which has experienced nearly continuous glacier retreat since the 1920s (Burns and Nolin, 2014; Georges, 2004; Rabatel et al., 2013). Regional ice loss on the order of 29% between 2000 and 2016

(Seehaus et al., 2019) has triggered cascading socioenvironmental repercussions spanning hydrographic shifts (Baraer et al., 2012; Bury et al., 2011; Mark et al., 2017) and changing geohazard exposure (Drenkhan et al., 2019; Huggel et al., 2020), among

40   others challenges. On longer timescales, glacier extents have fluctuated in accordance to the evolving tropical Andean paleoclimatic conditions, producing records of Quaternary climate history through the discontinuous moraine record (Stansell et al., 2022) as well as through continuous geologic proxies of ice extent (Rodbell et al., 2008).

Whether for interpreting the tropical glacial geologic record or understanding the trajectory of contemporary glacierized landscapes, disentangling the various drivers of glacier change is of primary concern. Like glaciers anywhere, those of the

45   tropics and CB are controlled to the first order by the prevailing (hydro)climatological conditions (Kaser, 2001; Kaser and Georges, 1999). Superimposed on these dominant forcings, additional processes differentiate rates of change across timescales and between individual sites. These processes include climatic ones, most notably the South American Summer Monsoon (SASM) system, which brings moisture across the Andes from the Amazon basin on a seasonal basis (Vuille et al., 2008b; Zhou and Lau, 1998). Driven by the annual migration of the Inter-Tropical Convergence Zone and the related South Atlantic

50   Convergence Zone (Kodama, 1992), the SASM produced stark hydroclimatic seasonality in outer-tropical latitudes, with over half of annual precipitation commonly occurring during DJF (wet-season) and negligible precipitation during JJA (dry-season). The El Niño-Southern Oscillation phenomenon (ENSO) modulates SASM strength while influencing temperature anomalies. The ENSO cycle is therefore a significant driver of inter-annual mass balance variability in the CB (Maussion et al., 2015; Vuille et al., 2008b).

55   Between individual glaciers, responses to climatic conditions are differentiated by morphometric factors such as hypsometry, aspect, and slope. Mass loss feedbacks associated with terrain radiation (e.g., Aubry-Wake and others, 2017) and glacial lake formation (e.g., King and others, 2018) further direct retreat patterns independently from climate. This latter factor has been shown to be particularly significant at the mountain range scale, where lake versus land terminating glaciers may respond differently to uniform climatic conditions (Brun et al., 2019). To interpret glacier responses to climate change, it is thus often

60   necessary to account for independent processes like lake formation alongside the climatic mass balance (e.g., Sutherland et al., 2020). A coupled mass balance and ice flow modeling approach is useful for parsing these diverse (climatic and non-climatic) influences over glacier change. Through transient simulations, coupled models can also facilitate interpolation between often discontinuous (paleo)glaciological observations.

However, tropical glaciers present persistent mass balance modeling challenges. One simple and common approach to glacier

65   mass balance modeling is the temperature-index (TI) model, which is built on the empirical relationship between surface temperature and a glacier's ablation rate (Hock, 2003). While the TI approach tends to perform well in the mid-latitudes, its applicability is less obvious in the tropics where the sensible heat flux plays a diminished role and melt does not immediately correlate with the continuously low temperatures (Fernández and Mark, 2016). However, there are compelling justifications for using TI models within the tropics. First, a practical data limit: the more rigorous approach of physical energy balance modeling

70   requires data which are not readily available at the spatiotemporal scale relevant to the topics outlined above. Moreover, temperature does tend to correlate with ablation on inter-annual to decadal timescales (Rabatel et al., 2013; Sicart et al., 2008), suggesting that a well calibrated TI model could theoretically internalize the numerous indirect impacts of temperature change (Ohmura, 2001).

The initial objective of our study is therefore to evaluate the performance of an empirical TI model in an outer-tropical context.

75   To do so, we present a case study of the CB's Queshque Glacier, simulating its evolution since 1962 using a coupled TI and ice

flow model. Our analysis yields insight concerning the dominant (hydro)climatic processes influencing glacier mass balance trends in the outer-tropical Andes. Furthermore, it illuminates how the transition from land to lake termination has impacted rates of glacier retreat, irrespective of climate.

2 Site Description

80   The Queshque Glacier (9.79˚S, 77.25˚W) is situated in the southern CB's Catac District and as of 2008, covered an area of 1.65 km^2 (Fig. 1a). From its headwall elevation of approximately 5460 m a.s.l., the glacier flows to the southwest, which provides optimal topographic shading, making it among the minority of glaciers in the range to retain a substantive ablation tongue. Located in the northern outer-tropical glacier region (Sagredo and Lowell, 2012), Queshque experiences the strong hydroclimatic seasonality described above and is therefore sensitive to fluctuations in the timing and intensity of moisture delivery by the

85   SASM. While the glacier's 20th century retreat trend can be explained by significant warming (Mark and Seltzer, 2005), interannual mass balance variability is likely related to the ENSO cycle and SASM dynamics. The present study revisits the topic of mass balance forcings of Queshque Glacier, incorporating new data, observations, and improved numerical modeling to investigate both climatic drivers of ice loss and the impacts of transitioning from land to a lake terminating conditions.
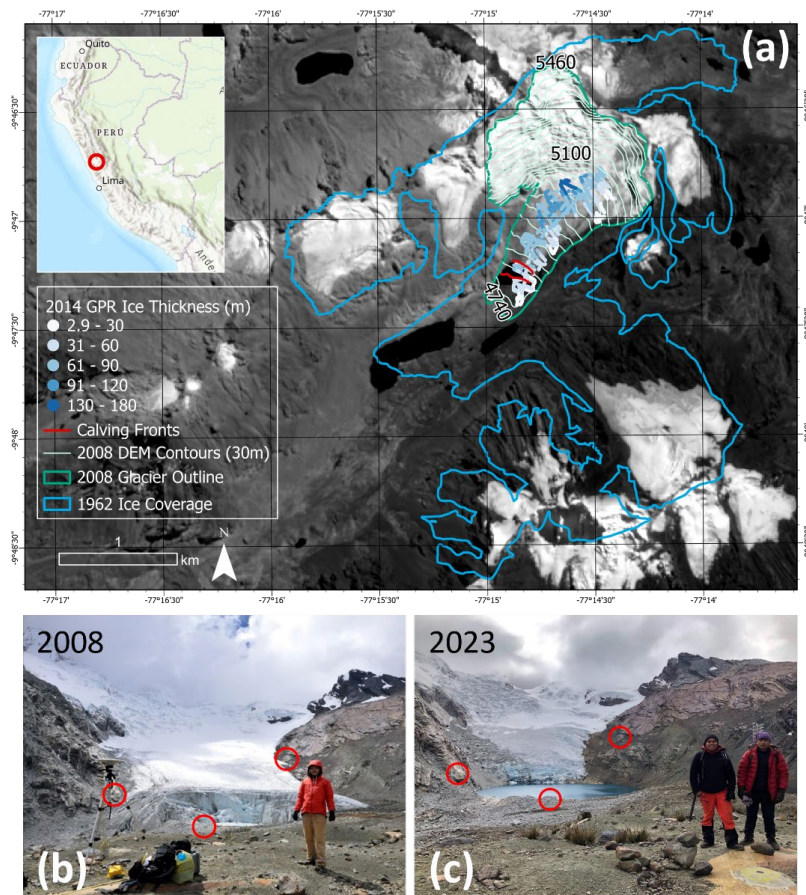
90 **Figure 1: Location of Queshque Glacier on base imagery from 2023 (Sentinel 2). The position of calving fronts in 2018**
and 2020 (derived from Sentinel 2 imagery) also shown. Inset basemap courtesy of ESRI (a). Field photos from 2008 (b)
and 2023 (c) are marked with stable reference points for comparison.

We follow Queshque's retreat history over two periods: 1962-2008 and 2008-2020. Between 1962 and 2008, Queshque retreated
over 1 km and ice coverage in the valley was dramatically reduced. From 2008 through 2020, the glacier retreated an additional

95 ~350 m and as of 2020, terminated at approximately 4800 m a.s.l. Retreat patterns after 2008 were modified by the onset of
frontal ablation into a new proglacial lake. Proglacial lake formation occurred in two phases. First, after 1990 a small lake
formed between the southern valley wall and the left lateral side of the glacier. By 2008, thinning and retreat had separated the
glacier from this lake, but a till-covered bedrock knob continued to dam the water above the ice terminus elevation. The lake
began draining towards the glacier, resulting in a mixture of outflow and meltwater pooling against the terminal ice (Fig 1b). The

100 second phase occurred after 2008, as further retreat revealed a significant overdeepening at the base of the glacier. Meltwater and
outflow from the perched lake have continued to fill this overdeepening, forming a sizeable bedrock and till-dammed proglacial
lake. As a result, lake calving became an observable component of total mass loss (Fig. 1c). By 2023, Sentinel 2 imagery shows
that the lake had grown to about 300 m in width and 450 m in length, covering an area of approximately 100,500 m^2.

3 Data and Methods

105 **3.1 Geodetic Mass Balance**

A geodetic mass balance measurement between the dry seasons of 1962 and 2008 is derived by differencing digital elevation
models (DEMs) from the respective years. Vertical aerial photographs taken on 12 July 1962 were used to produce a
stereographic model of the glacier and surrounding terrain and extract a digital restitution of discrete point elevations over the
glacier surface at a 30 m spacing using a Wild B8 analog plotter (i.e. Brecher and Thompson, 1993). Points were then mapped to

110 topographic contours at 25 m vertical resolution. A second DEM was produced using airborne LiDAR flown in July of 2008
(Huh et al., 2017). The LiDAR point cloud was converted to a 1 m resolution DEM covering the Queshque valley, used to
delineate the 2008 ice boundary, then resampled to a courser 10 m resolution for use in the glacier model.

After aligning the DEMs using 3-dimensional coregistration (see Supplement), we subtract the 1962 topography from that of
2008. We then calculate the specific (area averaged) mass balance (SMB) between 1962 and 2008 using projected pixels falling

115 within the 2008 glacier boundary by Eq. (1):

$$SMB = \frac{\rho_{water}}{\rho_{ice}}\frac{dxdy}{\Delta t}\sum_{i=1}^{n}\Delta h_i \qquad (1)$$

where dx and dy are the pixel resolution in the x and y dimensions of the local projection, Δt is the timespan in years, and Δh_i is
the elevation change for a given pixel of the n pixels within the 2008 glacier boundary. ρ_{water} and ρ_{ice} are the densities of water
and ice, taken respectively as 1000 and 900 kg m^{-3}.

120 **3.2 Glacier Bed Topography and Ice Thickness**

A ground penetrating radar (GPR) survey using 10 MHz frequency was conducted over the Queshque Glacier tongue during the
dry season of 2014 using the Radar HF from Unmanned Industrial LDTA (Fig. 1a). Coordinates and surface elevations
associated with the radar scans are established by averaging values from two GPS receivers. We interpreted radar scans visually
using RadarView 1.0 software and determined thickness profiles based on first reflectance. These values were subtracted from

125 the GPS ice surface heights to derive the bed topography. We calculated ice thickness in 2008 (derived thickness) by subtracting

the bed topography from the 2008 DEM. We then randomly divided the 2014 GPR survey into equally sized calibration and validation datasets before downscaling the respective subsets by averaging observations located within the same 10x10 m grid cell. This aggregation method facilitates comparisons between ice thickness observations and models without altering the spatial patterning of the GPR data (Pelto et al., 2020).

130   To ensure the accuracy of our derived thickness measurements, we evaluate them against a minimal GPR transect surveyed in 2009 (Stansell et al., 2022). For each point observation from the 2009 transect, we average the values from the four closest grid cells that contain derived thickness measurements. We then evaluate derived ice thickness error (derived minus observed thickness) on a point-by-point basis. Error ranges from 13 m to -15 m, with a single outlier of -28 m. Excluding the outlier, the datasets show strong agreement, with respective root mean squared error (RMSE), mean absolute error (MAE), and mean error

135   (ME) values of 7 m, 5 m, and ~0 m. While we would expect to detect modest (<0.5 m) thinning in the ablation zone between 2008 and 2009, the resolution of the GPR datasets may preclude this observation.

3.3 Climatology

The SENHAMI-HSR-PISCO (hereafter PISCO) monthly gridded temperature, precipitation, and fixed gridded reference altitude datasets are adopted for the period 1980-2020 (Aybar et al., 2020; Huerta et al., 2023). Mean monthly temperatures are estimated

140   by averaging the average minimum and maximum daily temperatures for each month. The PISCO climatology is extended to January 1960 using monthly temperature and precipitation standard anomalies from the downscaled Climate Research Unit (CRU) dataset (Harris et al., 2014; New et al., 2002). Both the PISCO and CRU datasets showcase typical outer-tropical Andean features, with stark precipitation seasonality (nearly all precipitation occurring during the austral summer) and only slight seasonal variation in temperature. Despite its higher spatial resolution, PISCO runs a local warm bias as compared to a

145   completely overlapping timeseries from CRU. Temperature and precipitation bias correction are addressed in the mass balance model calibration section.

3.4 Glacier Model

To evaluate drivers of glacier mass change and ice loss, we employ mass balance, ice flow, and calving models from the Open Global Glacier Model (OGGM) version 1.6.1 (Maussion et al., 2019). All simulations begin from the glacier state in 2008 and

150   leverage the altitude band approach to create a flowline-based representation of the glacier (Huss and Farinotti, 2012; Huss and Hock, 2018). The glacier is divided into equally spaced elevation bands at 20 m intervals (half the resolution of the underlying map) and mean glacier attributes are calculated per band, beginning with elevation, width, area, and slope, all of which are derived from the 2008 DEM and glacier outline. Calibration of the model components is described below. Constant and calibrated parameters are listed respectively in Tables 1 and 2.

155   ### 3.4.1 Mass Balance Model Ensemble

We employ the OGGM's monthly temperature index (TI) scheme using the extended PISCO climatology. The mass balance m during month i at elevation z is computed as:

$$m_i(z) = p_f P_i^{solid}(z) - \mu \max((T_i(z) + \varepsilon_T) - T_{melt}, 0) \tag{2}$$

where $P_i^{solid}(z)$ and $T_i(z)$ are the monthly solid precipitation and average monthly temperature at a given elevation, T_{melt} is the

160   temperature above which melt can occur, and μ is a positive degree-day factor (Hock, 2003). We assume orographic precipitation enhancement to be uniform across the glacier, allowing us to use a single precipitation factor (p_f) to scale P_i from the gridded

climatological dataset. All precipitation is assumed to be frozen when $T_i(z) < 0°C$ and liquid when $T_i(z) > 2°C$. At intermediate temperatures, the proportion of solid to liquid precipitation is scaled linearly. $T_i(z)$ is calculated using a lapse rate of -6.5°C for each km difference in altitude between a given point on the glacier and the climatology's reference altitude of 5111m. Due to the warm bias identified previously, temperature is further reduced by a negative temperature bias parameter (ε_T).

Annual modeled SMB is calculated by averaging the area weighted elevation band mass balance per month. Three free parameters, ε_T, μ, and p_f are calibrated by fitting modeled mass balance between 1962 and 2008 to the observed geodetic SMB. To do so, we vary ε_T by increments of 0.5°C between -9.0 °C and -6.5°C, producing six mass balance models with differing variances (climatic sensitivities), but uniform mean SMB during the calibration period. Because each subsequent modeling step depends on the mass balance parameters, the six parameter sets become the basis for a model ensemble used in the remainder of the study.

3.4.2 Glacier Thickness and Flow Model

We compute initial (2008) glacier ice thicknesses for each ensemble member following a well-documented continuity approach that leverages the calibrated mass balance models (Farinotti et al., 2009; Maussion et al., 2019). OGGM first evaluates the "apparent mass balance" ($\widetilde{m}$) per altitude band by assuming steady-state conditions (SMB=0). Ice flux (q) at each band is then calculated as the cumulative apparent mass balance from the area (a) above a given altitude (z). By continuity, we can assume that flux as cumulative mass balance above a given altitude band is balanced by ice flowing out of the band. OGGM therefore sets cumulative mass balance equal to ice flow using the shallow ice approximation (Hutter, 1981):

$$q = \int_z^{z_{max}} \widetilde{m}\, da = S * \frac{2A}{n+2} h(\rho_{ice} g h \alpha)^n \tag{3}$$

Where z_{max} is the maximum glacier altitude, S is elevation band width, g is the acceleration due to gravity, α is surface slope derived from the 2008 DEM, and h is ice thickness. A and n are the creep parameter and exponent from Glen's flow law, which describes the deformation of polycrystalline ice (Glen and Perutz, 1955). We adopt the conventional $n = 3$, and leave A as a free parameter. While total ice movement results from the combination of deformation ("creep") and basal sliding, data scarcity limits our ability to estimate sliding. We therefore assume that all flow arises from deformation. As a result, it is likely that our models overestimate the magnitude of deformation while accurately predicting ice flux.

OGGM performs a glacier ice thickness inversion by solving Eq. (3) for h at the center of each altitude band and extrapolating ice thickness by assuming a parabolic bed shape. The steady-state assumption can often lead to overestimated mass flux and therefore exaggerated overdeepenings located near the base of the glacier. To address this and achieve realistic proglacial lake depths, we set a minimum slope parameter of 7.5, which increases ice velocity at the expense of thickness.

We calibrate the A parameter during the inversion by minimizing ME in ice thickness against the GPR calibration dataset. Because the inversion is sensitive to the mass balance parameters, A is calibrated individually for each of the model ensemble members. After identifying an optimal A parameter for each member, we evaluate the resulting ice thickness map for ME and MAE against the GPR validation dataset.

For dynamic glacier simulations, we use the OGGM Flux-Based model based on Glen's flow law. For each model ensemble member, we therefore adopt the respective A parameter calibrated during the inversion and continue to neglect sliding.

3.4.3 Calving Model

The OGGM implements a simple scheme developed by Oerlemans and Nick (2005) for calculating the calving flux ($q_{calving}$) at lake terminating glaciers:

$$q_{calving} = kdh_f w \tag{4}$$

where k is a calving rate constant, h_f is ice thickness at the calving front, and w is the width of the calving front. The d parameter is the water depth calculated from the water level (z_w) and bed altitude at the glacier terminus (z_b) as:

$$d = z_w - z_b \tag{5}$$

While z_w may vary on a seasonal basis, an examination of satellite imagery shows negligible variation in the ice distal extent of surface water between the small pool visible in 2008 and the sizeable lake present in 2020. We therefore adopt the DEM altitude at the site of pooling in 2008 as a constant z_w throughout the duration of the study. z_b is adjusted each month based on the position of the calving front and k is adopted from a low-end estimate used in previous work (Table 1).

Name (unit)	Symbol	Value	Source
Melt Threshold (°C)	T_{melt}	-1.0	Maussion et al. (2019)
Glen's Exponent	n	3	Maussion et al. (2019)
Calving Rate Constant (a^{-1})	k	1.2	Oerlemans and Nick (2005)
Water Level (m a.s.l.)	z_w	4727	Sentinel 2 Imagery

Table 1: Constant model parameters used in Eqs. (1-5).

3.5 Glacier Evolution Experiments

We run four dynamic ice flow modeling experiments to evaluate the relative drivers of ice loss from 2008 through 2020. To isolate the impact of frontal ablation, we force the glacier to evolve with and without lake calving under the historical climatology (sec. 3.3), for which we take the PISCO dataset between 2008 and 2020. The two additional experiments both neglect calving and isolate the temperature versus precipitation forcings by maintaining the monthly climatological temperature or precipitation levels as recorded during the first 30 years of the mass balance record (1962-1991). Experiments are performed independently for each of the six model ensemble members and the results are validated against glacier surface velocity measurements representative of 2017-2018 (Millan et al., 2022).

4 Results

4.1 Mass Balance Model Calibration

After aligning the 1962 and 2008 DEMs through 3-dimensional coregistration (see Supplement), differencing the DEMs shows that Queshque experienced a SMB rate of -442 mm w.e. a^{-1} between the two periods. This value provides a constraint on mean modeled SMB for each ensemble member throughout the calibration period, resulting in higher μ as ε_T becomes more negative (Table 2). As a result, models with low magnitude ε_T have less interannual SMB variability and we can therefore characterize them as lower climate sensitivity models. Alternatively, high magnitude ε_T models showcase greater variability, or higher climate sensitivity (Table. 2). While modifying the p_f parameter leads to intuitive changes in climate sensitivity (higher values increasing sensitivity to temperature as compensation), doing so does not provide additional insight into the mass balance regime. Lacking meteorological data to identify the "correct" p_f parameter, we opt for a constant of 2.5, which is commonly adopted when using the CRU gridded precipitation product in glaciological applications (Marzeion et al., 2012; Maussion et al., 2019).

Parameter		(low sensitivity) - Model Number - (high sensitivity)					
Name (unit)	Symbol	1	2	3	4	5	6
Temperature Bias (˚C)	ε_T	-6.5	-7.0	-7.5	-8.0	-8.5	-9.0
Precipitation Factor	p_f	2.5	2.5	2.5	2.5	2.5	2.5
Degree-Day Factor (kg m^{-2} d^{-1} ˚C^{-1})	μ	1.74	2.58	3.87	5.92	9.31	15.31
Creep Parameter (10^{-24} Pa^{-3}s^{-1})	A	2.78	3.57	4.42	5.34	6.30	7.31

Table 2: Calibrated model parameters used in Eqs. (2-3) for six-model ensemble.

4.2 Climate and Mass Balance Variability

230   We use the Mann-Kendall test to identify significant (p<0.05) linear trends in the climate and mass balance timeseries. Over the course of the mass balance simulation period (1962-2020), mean annual temperature (MAT) rose by approximately 0.15˚C per decade based on a simple linear regression, with dry-season temperatures rising faster and more consistently than during the wet-season (Fig. S4a). While we detect no significant trend in total annual precipitation (TAP), a moderate, though statistically insignificant drying (wetting) trend is present during the dry (wet) season (Fig. S4b). These trends were associated with a model

235   ensemble average SMB decline of approximately -221 mm w.e. a^{-1} per decade by 2020.

     To evaluate the relationship between glacier mass balance variability, temperature, precipitation, and ENSO, we detrend and normalize all climate and mass balance variables by fitting them to 3rd order polynomials, subtracting the polynomial from the respective timeseries, then dividing the detrended data by their standard deviations. We then use Pearson correlations to compare the normalized SMB and climate timeseries to the ENSO indices including Niño-3.4, the Oceanographic Niño Index (ONI), the

240   Southern Oscillation Index (SOI), and their seasonal values. All correlation coefficients reported are within a confidence interval of p<0.05. We find that SMB is tightly correlated with MAT (r = -0.93) (Fig. 2a). TAP maintains a moderate correlation with SMB throughout the simulation, increasing after 1991 to a correlation coefficient of 0.59. Correlations also suggest that SMB is slightly more closely linked to dry-season than it is to wet-season precipitation (Fig. 2b). Regarding ENSO, the most consistent predictor of annual mass balance is the wet-season Niño-3.4, which retains a strong anticorrelation with SMB throughout the

245   duration of study (r< -0.70). While annual Niño-3.4 values serve as a moderate SMB predictor during the first 30 years after 1962, this relation appears to dampen over time, becoming insignificant in the latter 30-year period. Alternatively, negative correlations with the wet-season ONI index reaches -0.86 in the last 30 years of the study period. Other indices appear to reverse in the sign of their correlation with SMB over the course of the study. Most notably, the dry season SOI index maintains a moderate positive correlation with SMB for the first 30 years before switching to a low to moderate (though not statistically

250   significant) negative correlation after 1991 (Fig. 2c).
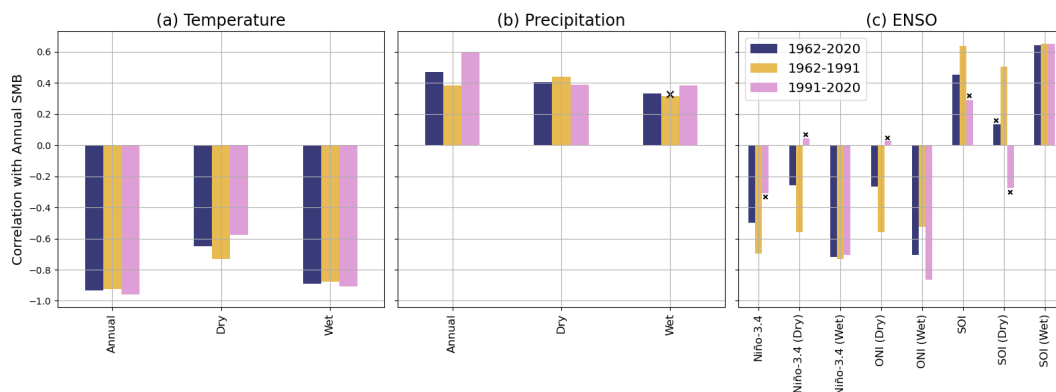
Figure 2: Correlations for annual, dry-season (JJA), and wet-season (DJF) detrended temperature (a), precipitation (b), and ENSO indices (c) with detrended annual SMB. Insignificant correlations (p>0.05) are marked by crosses.

4.3 Climate and Mass Balance Seasonality

255 We evaluate monthly accumulation and ablation variability between 2008 and 2020, showing that the model reproduces an archetypical tropical glacier mass balance regime. Accumulation, taken as the total solid precipitation to fall on the glacier each month, follows the pattern controlled by the SASM. Across all models, 53-56% of accumulation between 2008 and 2020 fell during the wet season, while less than 2% occurred in the dry season (Fig. S5a). Following a similar though less pronounced pattern, 27-32% of all ablation occurred during the wet season, while 19-22% occurred in the dry season (Fig. S5b). Together,

260 this seasonality produces a mass balance regime wherein ablation occurs continuously throughout the year but enhances during the wet season when virtually all accumulation occurs. As a result, the model produces consistent negative mass balance between May and November, with the exception of November 2010, which had a slight positive balance due to above average accumulation and below average temperature. Both positive and negative mass balance months occur between December and April and the net balance magnitudes are greater during this time (Fig. 3). As model sensitivity increases, accumulation and

265 ablation seasonality are amplified, and net balance becomes increasingly variable.
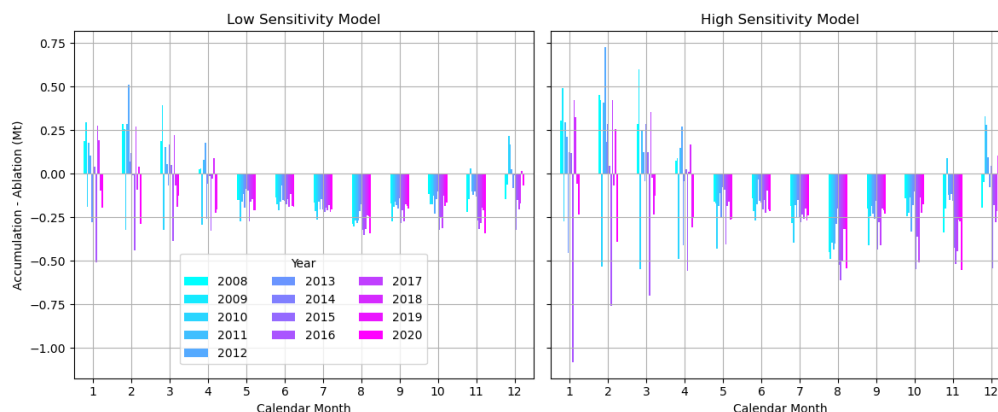
Figure 3: Net mass balance as accumulation minus ablation for each month of each year (2008-2020). The low (left) and high (right) sensitivity models correspond to model numbers 2 and 5, respectively.

4.4 Glacier Volume and Thickness Estimates

270 Due to the ice thickness inversion procedure's dependence on the mass balance parameters, the inverted bed topography differs across models, leading to differences in total glacier volume. Below 5100 m, however, ice thickness is constrained by the GPR observations. Model results at lower elevations are therefore consistent to one another, with mean thickness ranging negligibly between 73.5 and 73.6 m. Error against the validation GPR dataset is also consistent, with approximately 30 cm ME and 24 – 25 m MAE (Table 3). These metrics imply that while ice thickness at any given point is likely to be over or underestimated by about

275 25 m, the average ice thickness and therefore glacier volume is well constrained. This level of accuracy is comparable to similar work using GPR (Pelto et al., 2020). By contrast, observations are lacking in the accumulation zone, and ice thickness varies across models. Initial modeled ice volumes range from $7.7\text{-}8.1\times10^7$ m^3, reducing as climatic sensitivity increases. Relatedly, the calibrated creep parameter, A, increases with greater climate sensitivity, reflecting enhanced ice flux (Table 2).

Model Number	Validation ME (m)	Validation MAE (m)	Initial Ice Volume (10^7 m^3)	Mean Ablation Zone Thickness (m)
1 (Least Climate Sensitive)	0.29	24.01	8.10	73.6
2	0.29	24.18	8.02	73.6
3	0.30	24.37	7.95	73.6
4	0.30	24.56	7.88	73.5
5	0.31	24.81	7.81	73.5
6 (Most Climate Sensitive)	0.32	25.14	7.74	73.5

Table 3: Ice thickness inversion results for each model ensemble member.

280 **4.5 Ice Dynamics**

The four glacier evolution experiments isolate different mass balance forcings, enabling us to parse their relative influences over glacier dynamics. Forced by the real-time monthly conditions recorded over the study period, the ensemble mean glacier volume reduces by 26±6% between 2008 and 2020. Holding monthly precipitation to climatological means from 1962-1992 but retaining the recorded temperature values results in a similar trend with heightened volume loss of 30±6%. Alternatively, driving the

285 model with climatological temperature and real-time precipitation yields a nearly steady-state ensemble mean volume, with more climatically sensitive models producing net glacier growth of up to nearly 8% (Fig. 4a). Finally, incorporating the effects of proglacial lake formation by implementing frontal ablation accelerates mass loss beginning in 2010 and produces a narrower model spread of 28-33% volume loss by 2020 (Fig. 4b).

A comparison between modeled and observed ice velocity profiles suggests that the model produces realistic local ice dynamics.

290 Both models and observations show glacier velocity in 2018 increasing from a minimum at the beginning of the flowline (the top of the glacier), peaking at around 900 m downstream, then decelerating. Surface velocities spike again at the calving front (Fig. 5). In terms of magnitude, models 2, 3, and 4 stay truest to observed velocities, though each overestimates the peak velocity at the glacier terminus. An apparent positive terminus velocity bias is present in most models, which is likely related to the impact of lake depth on calving flux. Because higher climate sensitivity models retreat faster when excluding calving, the addition of a

295 calving mechanism has a greater impact on lower sensitivity models, bringing the ensemble spread of total volume loss closer together. By 2018, the higher sensitivity models retreat to a greater extent than their less sensitive counterparts. However, differences between models with calving are reduced as compared to when neglecting this process (Fig. 6).
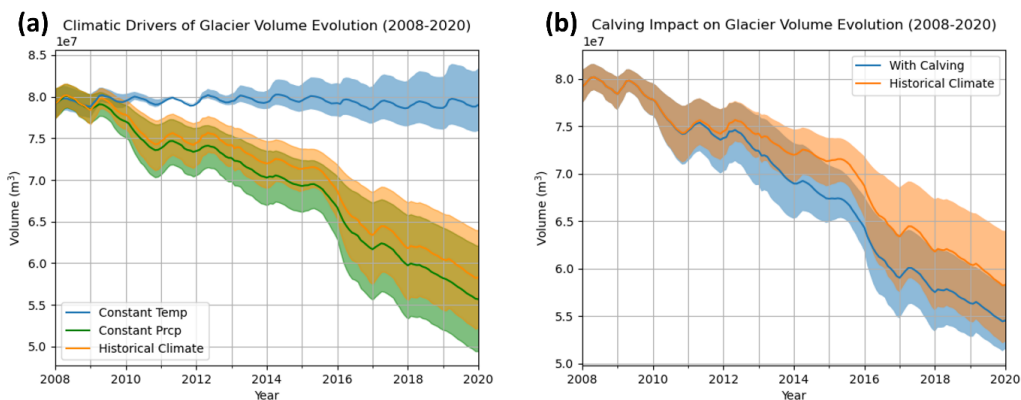
Figure 4: Comparison of dynamic glacier evolution under the historical climate, constant climatological mean temperature, and constant climatological mean precipitation (a). Comparison of glacier evolution under the historical climate conditions with and without including frontal ablation (b). Shaded regions indicate the model ensemble spread.
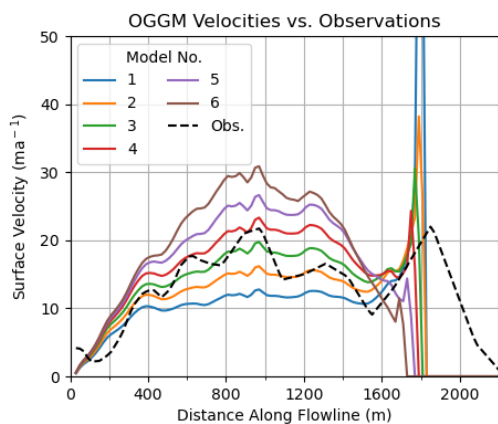
Figure 5: Surface velocity profiles of the 6-member model ensemble. Observations (Obs.) come from Millan et al. (2022). Modeled velocity falls to zero at glacier terminus whereas observations reduce more gradually, owing to satellite image resolution and potentially the presence of ice mélange.
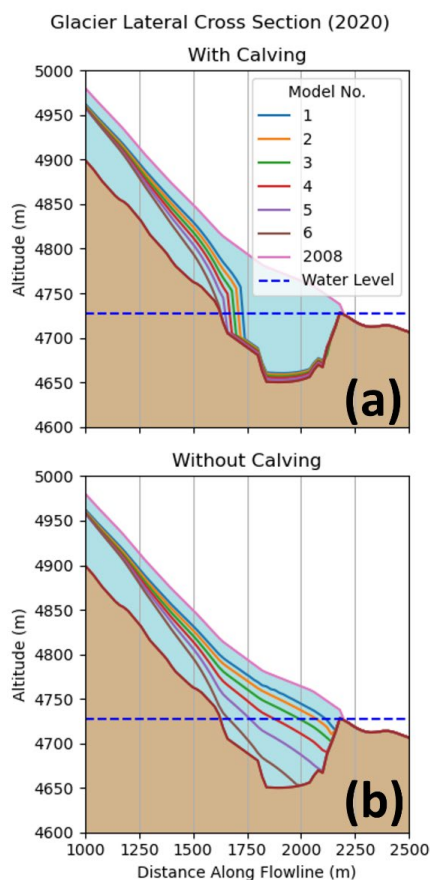
Figure 6: Details of the glacier lateral cross section in 2020 produced by each model ensemble member with (a) and without (b) calving. The ice surface in 2008 is depicted in pink. Note that the x and y axes are not to scale, and that the first 1000 m of the glacier are excluded to highlight differences at the glacier terminus.

310 **5 Discussion**

5.1 Tropical Glacier Mass Balance: Major Components Reproduced in TI Model

From a climatological perspective, the distinguishing feature of the outer-tropical glacier mass balance regime is the absence of strong thermal seasonality coupled with pronounced seasonal differences in precipitation (Kaser and Osmaston, 2002). This leads to continuous ablation throughout the year, with accumulation confined almost exclusively to the wet season. The magnitude of
315 ablation, however, is controlled by processes governing the net radiation balance and the partitioning of energy available for melt (Hastenrath, 1997). Multiple factors influence this partitioning, but generally results in an archetypical outer-tropical Andean glacier seasonality featuring enhanced ablation during the wet season (Kaser and Georges, 1999). Glacio-hydrological observations at Yanamarey and Uruashraju in the CB support this theory, showing that net accumulation occurred only during JFMAM, and JFMA, respectively (Mark and Seltzer, 2003). Further confirmation is offered by process-based surface energy
320 balance (SEB) models applied on glaciers in the CB (Fyffe et al., 2021) and Bolivia's Zongo Glacier (Sicart et al., 2005; Wagnon et al., 1999) which show that energy for melt typically peaks during the wet season. The persistent exception is the CB's Shallap

Glacier, where continuous snowpack (higher albedo) tends to decrease energy available for melt during the wet season (Fyffe et al., 2021; Gurgiser et al., 2013). Whereas an enhanced latent heat flux reduces dry season melting in the drier Bolivian glaciers (e.g., Wagnon and others, 1999), in the CB, this process appears to be secondary to those controlling the shortwave energy

325 balance, particularly through various albedo feedbacks (Fyffe et al., 2021). Regardless of the dominating process, wet season mass balance in the outer-tropics tends to be more variable than during the dry season (e.g., Maussion and others, 2015), resulting in close coupling between the annual SMB and wet season hydroclimatology (Vuille et al., 2008a).

These theoretical and observed features of tropical glacier seasonality are reproduced in the present study despite key processes being excluded by nature of the TI approach (Fig. 3, A5b). Namely, our model does not include the all-wave radiation balance

330 nor latent heat flux, and therefore neglects the critical roles of albedo, cloudiness, and potentially, sublimation. Nonetheless, Fig. S5 shows that ablation minimizes during the dry months (particularly MJJ) and that while the wet season mass balance is highly variable, net accumulation occurs exclusively during this time. The increase in ablation during August is due to consistently warmer August temperatures in the PISCO climatology.

In summary, our results using a TI approach reproduce the expected outer-tropical Andean mass balance seasonality despite

335 lacking fully resolved physical processes. In our case, the slight cooling evident during the dry season suffices to reduce the magnitude and extent of melt across the ablation zone, producing a SMB seasonality that is enhanced in the high climate sensitivity model realizations. Where glaciers exhibit reduced gradients in albedo and therefore atypical ablation seasonality (e.g., Shallap), or where the latent heat flux plays a more significant role (e.g., Quelccaya or Zongo) our model would be unlikely to reproduce the observed mass balance regime due to the heightened significance of energy fluxes which we neglect. An

340 enhanced TI (ETI) approach considering the radiation balance in addition to temperature (Pellicciotti et al., 2005), could improve model reliability in these settings. The single study evaluating this method on a tropical glacier (Zongo) shows that as expected, a locally calibrated ETI model outperforms a basic TI approach over a one-year study period (Fuchs et al., 2016). While the authors do not rigorously calibrate their basic TI model, the TI approach also reproduces the observed seasonality in glacial discharge. We propose in agreement with previous work (Sicart et al., 2008) that while on shorter timescales their accuracy is

345 limited, on inter-annual to decadal timescales TI models are suitable for predicting glacier evolution in certain outer-tropical glacier settings. This permits an assessment of the multi-decadal relationship between Queshque Glacier's mass balance and hydroclimatological trends.

5.2 Hydroclimate Trends: Recent Precipitation Levels Dull Impact of Warming

Beyond the overall 1962-2020 warming trend of 0.15°C per decade, we detect significant MAT warming trends in nearly every

350 30-year period beginning in 1967. Based on a rolling 30-year period, warming rates peak around 1974 at close to 0.30°C per decade and, while remaining positive, decline until the final period of 1991-2020. Rates appear to be more statistically significant during the dry season as compared to the wet season (Fig. S4a). In comparison, we detect a visual, though not statistically significant, trend towards wetter conditions throughout the study period, particularly during the wet season (Fig. S4b). Lacking significance in the precipitation trends, we draw no conclusions regarding their impact on glacier mass balance.

355 However, our glacier evolution experiments also indicate that precipitation levels in the latter study period (2008-2020) served as a positive mass balance forcing, dampening the ice volume loss that would have taken place should the monthly averages from 1962-1991 have persisted into the 21st century. The opposite experiment (holding temperatures at the mean monthly values from 1962-1991 while maintaining recent precipitation levels) shows that modern precipitation would allow Queshque to remain in relative equilibrium with the mid-to-late 20th century temperature (Fig. 4a).

360 Despite constraining our geographic scope to the immediate vicinity of Queshque Glacier and limiting our climatological analysis to a single data source, our results mirror those of previous studies while contributing a closer analysis of direct impacts to a tropical glacier. Mark and Seltzer (2005) combined meteorological station data from the CB region to construct a temperature and precipitation timeseries against which to compare observed ice loss on Queshque and the neighboring glaciers. Their analysis, which concerns the period from 1951 to 1999, finds that warming persisted throughout the study period, though

365 warming rates declined over time. They find no significant trend in precipitation. More recently Schauwecker and others (2014) collated an expanded set of meteorological observations and identified the same slowing (though persistently positive) warming trend. They also identify a shift to higher precipitation totals beginning in 1993. This latter study concludes that recent ice loss is not consistent with the simultaneous reduction in the warming rate and increase in precipitation. They propose instead that glacier retreat is a disequilibrium response. Alternatively, the former study (Mark and Seltzer, 2005), concludes that the

370 magnitude and geometry of observed ice loss is consistent with a warming explanation. Our results support this argument, showing that recent precipitation levels reduced ice loss rates, but that the retreat trajectory was dominated by the trend in temperature (Fig. 4a).

5.3 Mass Balance Variability: Wet-Season ENSO Signal Linked to Annual SMB Anomaly

Numerous studies have previously investigated the role of ENSO in regulating interannual variability in tropical Andean glacier

375 mass balance, finding that El Niño years tend to produce negative mass balance anomalies while La Niña has the opposite effect (Kaser et al., 2003; Maussion et al., 2015; Vuille et al., 2008b). In agreement with these studies, we find that ENSO has a greater impact on temperature than precipitation, as the latter is controlled primarily by easterly advection from the Amazon basin, which is less directly tied to Pacific sea-surface temperatures (SST). Kaser et al. (2003) find a general correlation between SOI and the hydrological balance of CB glaciers. Their timeseries is used by Vuille et al. (2008b), who find a significant negative

380 correlation between Niño-3.4 SST and mass balance, though the relationship degrades during the latter 20th century. Maussion et al. (2015) confirm this relationship, finding even stronger anticorrelations, albeit on a single glacier in the CB (Shallap). They propose that the Niño/warm signal is the dominating factor influencing the anticorrelation with annual SMB, but primarily due to impacts on the snow-to-rain ratio, and therefore on the glacier surface albedo and shortwave balance. They find ENSO influence over total precipitation to be less systematic.

385 Our analysis of the detrended mass balance and climatological timeseries in relation to conventional ENSO indices offers additional insight. As reported above, we find that the relationship between most ENSO indices and the annual SMB anomaly reduces in the latter half of the study period (Fig. 2c). While verifying this observation warrants further investigation, we find that a strong SMB-ENSO relationship persists over all three periods (first 30 years, last 30 years, entire timeseries) when considering wet season ENSO intensity alone. Despite our model showing slightly higher SMB correlations with dry versus wet

390 season precipitation during all but the most recent period (Fig. 2b), this finding supports the conclusion that wet season dynamics are the most important predictors of annual outer-tropical glacier mass balance (Fyffe et al., 2021; Vuille et al., 2008a). Furthermore, the stronger relationship between ENSO and temperature (as opposed to precipitation) implies that given ample moisture, wet season temperature, by modifying the snow-to-rain ratio and determining the magnitude of ablation at lower altitudes, plays a key role in modulating inter-annual mass balance variability. This is supported by the stronger modeled

395 correlations between annual SMB and temperature during the wet season as compared to the dry season (Fig. 2a). It is notable that despite neglecting the critical albedo effect, the relationships described above are produced using a TI approach.

5.4 Climatic Decoupling: Proglacial Lakes Accelerate Retreat and Decrease Variability Between Retreating Glaciers

It has been widely recognized that frontal ablation in lake terminating glaciers alters the patterns and rates of mountain glacier retreat (Brun et al., 2019; Carrivick and Tweed, 2013; Chernos et al., 2016; Sutherland et al., 2020), and recent work has

400   observed widespread acceleration of ice loss as glaciers transition from land to lake terminating states (King et al., 2018, 2019; Sato et al., 2022). Our numerical modeling results support these assessments, showing that the advent of frontal ablation led to enhanced mass loss during the period from 2008 through 2020. After 2014, the mass loss from the least sensitive calving glaciers surpasses that of the ensemble mean of non-calving glaciers. Less trivially, while volume loss rate variability of both the calving and non-calving realizations appear to follow trends dictated by the climatic conditions, the ensemble spread varies less when

405   calving is included and deviation between calving ensemble members is reduced. This reduction is primarily caused by enhanced ice loss from the calving glaciers with the lowest climatic sensitivities, suggesting that the initiation of the calving process locks the glacier into a climatically independent mass loss trajectory.

Though the present study considers only a single glacier with an uncertain climate-mass balance relationship, these results shed light on variability, or lack thereof, in mass loss observations on a regional basis. Observational studies have shown that among

410   other variables, differences in glacier hypsometry (Guha and Tiwari, 2023; Tangborn et al., 1990) and aspect (Abdullah et al., 2020) can alter the dominant accumulation and ablation processes and significantly impact the sensitivities of individual glaciers to a homogenous regional climate (Abdullah et al., 2020; Guha and Tiwari, 2023). As lakes proliferate across the deglaciating regions of the world (Shugar et al., 2020), our results indicate that the lower sensitivity preserving some glaciers may be counteracted by the equalizing and accelerating effect of frontal ablation.

415   While offering these general insights, the calving scheme representation used in the present study is simplified, and therefore limited in accuracy and precision. Sensitive to lake depth, the model accuracy is dependent on the bed height derived during the ice thickness inversion. It is likely that the magnitude of the bed depression is overestimated due to the equilibrium assumption enforced during the inversion procedure. As a result, we overestimate lake depth, and potentially the calving flux. This may explain why models with calving tend to overestimate the terminus ice velocity and linear retreat rate (Fig. 5).

420   Calculated along the glacier flowline, modeled lake depth reaches a maximum of 67-77 m, averaging at 46-53 m, depending on the model realization. These values are similar to maximum and mean measured depths of 73 m and 34 m from the nearby (9.39˚S, 77.38˚W) Lake Palcacocha (Muñoz et al., 2020). To further evaluate our modeled lake profile, we estimate expected mean lake depth using established, though highly uncertain, lake geometry-to-depth scaling techniques. From the width-to-depth relationship presented by Muñoz et al. (2020), we can estimate a mean lake depth of 12.3 m. Alternatively, surface area-to-depth

425   scaling ratios for all regional lakes and for mixed dam-type lakes alone, suggest likely mean depths of 36 and 27 m, respectively (Wood et al., 2021). Considering that average depth along the lake's long axis is likely to exceed the area averaged depth over the entire lake, our estimated depth is not outside the realm of possibility. With this said, it is likely an overestimate. While this limits the accuracy of our calving model due to the linear relationship between lake depth and modeled calving flux, Fig. 5 shows that it does not result in highly overexaggerated rates of glacier retreat.

430   **6 Conclusions**

We have applied a long-term geodetic mass balance observation, an ice thickness survey, a high-resolution DEM, and new climatological data to calibrate and validate the ice flow and mass balance models from OGGM v. 1.6.1 in the context of a glacier located in the outer-tropical Andes. Our ensemble approach reflects the uncertain relationship between gridded climate data and actual conditions at the site of the glacier, which determine the model sensitivity of glacier ablation to changes in

435   temperature. After calibrating the ensemble members to fit observed mass loss between 1962 and 2008, we examine the

simulated SMB timeseries extended through 2020. We further implement an ice flow and lake calving model to more carefully study glaciological dynamics between 2008 and 2020, making use of the extensive GPR survey. Our results show that the simple TI mass balance model outperforms theoretical expectations despite neglecting key processes controlling tropical glacier ablation. Dynamic ice flow simulations show that between 2008 and 2020, warming and frontal ablation led to the mass loss of

440   about 31% and that this figure would have been enhanced if not for a relative increase in precipitation during this time. Furthermore, we find that inter-annual SMB variability since 1962 has been closely tied to the ENSO phase, most significantly during the wet season. Indeed, the overall annual SMB correlation with ENSO indices reduces over the course of the study period but remains strong during DJF. Finally, we find that the transition from land to lake termination not only accelerates glacier loss but reduces the variability between glaciers with otherwise different climatic sensitivities. Together, these findings

445   shed light on the processes influencing spatiotemporal variability in outer-tropical glacier mass loss and provide insight into the potential uses of empirical glacier models where complete meteorological data are lacking. Future research can apply similar methods to evaluate past and future tropical glaciological change over longer timescales.

Supplement

Supplementary material contains additional figures and text concerning DEM coregistration.

450   **Data Availability**

Code to reproduce all figures is available upon request.

Author Contributions

TYS designed the study and wrote the majority of text. BGM and NDS contributed to study design and writing. RCE conducted GPR fieldwork and data processing. HHB performed photogrammetry. BY and FSS contributed datasets used in the study and

455   ZL contributed to study design.

Competing Interests

The authors declare that they have no conflict of interest.

Acknowledgements

Author Henry H. Brecher passed away on 27 July 2024 during the composition of this manuscript, marking the end of a career in

460   the cryospheric sciences spanning over six decades. We honor the contributions he made to this study and to the field more broadly. We also acknowledge support from the National Science Foundation (grant EAR-2002541) and The Ohio State University Department of Geography. Additionally, we thank Adam Clark for his support with GPR as a master's student at the University of Montana in 2009. Finally, we thank the Peruvian Autoridad Nacional del Agua for their collegial support.

References

465   Abdullah, T., Romshoo, S. A., and Rashid, I.: The satellite observed glacier mass changes over the Upper Indus Basin during 2000–2012, Sci. Rep., 10, 14285, https://doi.org/10.1038/s41598-020-71281-7, 2020.

Aubry-Wake, C., ZÉPhir, D., Baraer, M., McKenzie, J. M., and Mark, B. G.: Importance of longwave emissions from adjacent terrain on patterns of tropical glacier melt and recession, J. Glaciol., 64, 49–60, https://doi.org/10.1017/jog.2017.85, 2017.

470   Aybar, C., Fernández, C., Huerta, A., Lavado, W., Vega, F., and Felipe-Obando, O.: Construction of a high-resolution gridded rainfall dataset for Peru from 1981 to the present day, Hydrol. Sci. J., 65, 770–785, https://doi.org/10.1080/02626667.2019.1649411, 2020.

Baraer, M., Mark, B. G., McKenzie, J. M., Condom, T., Bury, J., Huh, K.-I., Portocarrero, C., Gómez, J., and Rathay, S.: Glacier recession and water resources in Peru's Cordillera Blanca, J. Glaciol., 58, 134–150, https://doi.org/10.3189/2012JoG11J186, 2012.

475   Brecher, H. H. and Thompson, L. G.: Measurement of the Retreat of Qori Kalis Glacier in the Tropical Andes of Peru by Terrestrial Photogrammetry, Photogramm. Eng. Remote Sens., 59, 1017–1022, 1993.

Brun, F., Wagnon, P., Berthier, E., Jomelli, V., Maharjan, S. B., Shrestha, F., and Kraaijenbrink, P. D. A.: Heterogeneous Influence of Glacier Morphology on the Mass Balance Variability in High Mountain Asia, J. Geophys. Res. Earth Surf., 124, 1331–1345, https://doi.org/10.1029/2018JF004838, 2019.

480   Burns, P. and Nolin, A.: Using atmospherically-corrected Landsat imagery to measure glacier area change in the Cordillera Blanca, Peru from 1987 to 2010, Remote Sens. Environ., 140, 165–178, https://doi.org/10.1016/j.rse.2013.08.026, 2014.

Bury, J. T., Mark, B. G., McKenzie, J. M., French, A., Baraer, M., Huh, K. I., Zapata Luyo, M. A., and Gómez López, R. J.: Glacier recession and human vulnerability in the Yanamarey watershed of the Cordillera Blanca, Peru, Clim. Change, 105, 179–206, https://doi.org/10.1007/s10584-010-9870-1, 2011.

485   Carrivick, J. L. and Tweed, F. S.: Proglacial lakes: character, behaviour and geological importance, Quat. Sci. Rev., 78, 34–52, https://doi.org/10.1016/j.quascirev.2013.07.028, 2013.

Chernos, M., Koppes, M., and Moore, R. D.: Ablation from calving and surface melt at lake-terminating Bridge Glacier, British Columbia, 1984–2013, The Cryosphere, 10, 87–102, https://doi.org/10.5194/tc-10-87-2016, 2016.

Drenkhan, F., Huggel, C., Guardamino, L., and Haeberli, W.: Managing risks and future options from new lakes in the
490   deglaciating Andes of Peru: The example of the Vilcanota-Urubamba basin, Sci. Total Environ., 665, 465–483, https://doi.org/10.1016/j.scitotenv.2019.02.070, 2019.

Farinotti, D., Huss, M., Bauder, A., Funk, M., and Truffer, M.: A method to estimate the ice volume and ice-thickness distribution of alpine glaciers, J. Glaciol., 55, 422–430, https://doi.org/10.3189/002214309788816759, 2009.

Fernández, A. and Mark, B. G.: Modeling modern glacier response to climate changes along the Andes Cordillera: A multiscale
495   review, J. Adv. Model. Earth Syst., 8, 467–495, https://doi.org/10.1002/2015MS000482, 2016.

Fuchs, P., Asaoka, Y., and Kazama, S.: Modelling melt, runoff, and mass balance of a tropical glacier in the Bolivian Andes using an enhanced temperature-index model, Hydrol. Res. Lett., 10, 51–59, https://doi.org/10.3178/hrl.10.51, 2016.

Fyffe, C. L., Potter, E., Fugger, S., Orr, A., Fatichi, S., Loarte, E., Medina, K., Hellström, R. Å., Bernat, M., Aubry-Wake, C., Gurgiser, W., Perry, L. B., Suarez, W., Quincey, D. J., and Pellicciotti, F.: The Energy and Mass Balance of Peruvian Glaciers, J.
500   Geophys. Res. Atmospheres, 126, e2021JD034911, https://doi.org/10.1029/2021JD034911, 2021.

Georges, C.: 20th-Century Glacier Fluctuations in the Tropical Cordillera Blanca, Perú, Arct. Antarct. Alp. Res., 36, 100–107, 2004.

Glen, J. W. and Perutz, M. F.: The creep of polycrystalline ice, Proc. R. Soc. Lond. Ser. Math. Phys. Sci., 228, 519–538, https://doi.org/10.1098/rspa.1955.0066, 1955.

505   Guha, S. and Tiwari, R. K.: Analyzing geomorphological and topographical controls for the heterogeneous glacier mass balance in the Sikkim Himalayas, J. Mt. Sci., 20, 1854–1864, https://doi.org/10.1007/s11629-022-7829-0, 2023.

Gurgiser, W., Marzeion, B., Nicholson, L., Ortner, M., and Kaser, G.: Modeling energy and mass balance of Shallap Glacier, Peru, The Cryosphere, 7, 1787–1802, https://doi.org/10.5194/tc-7-1787-2013, 2013.

Harris, I., Jones, P. D., Osborn, T. J., and Lister, D. H.: Updated high-resolution grids of monthly climatic observations – the
510   CRU TS3.10 Dataset, Int. J. Climatol., 34, 623–642, https://doi.org/10.1002/joc.3711, 2014.

Hastenrath, S.: Measurements of diurnal heat exchange on the Quelccaya Ice Cap, Peruvian Andes, Meteorol. Atmospheric Phys., 62, 71–78, https://doi.org/10.1007/BF01037480, 1997.

Hock, R.: Temperature index melt modelling in mountain areas, J. Hydrol., 282, 104–115, https://doi.org/10.1016/S0022-1694(03)00257-9, 2003.

515   Huerta, A., Aybar, C., Imfeld, N., Correa, K., Felipe-Obando, O., Rau, P., Drenkhan, F., and Lavado-Casimiro, W.: High-resolution grids of daily air temperature for Peru - the new PISCOt v1.2 dataset, Sci. Data, 10, 847, https://doi.org/10.1038/s41597-023-02777-w, 2023.

Huggel, C., Carey, M., Emmer, A., Frey, H., Walker-Crawford, N., and Wallimann-Helmer, I.: Anthropogenic climate change and glacier lake outburst flood risk: Local and global drivers and responsibilities for the case of lake Palcacocha, Peru, Nat. Hazards
520   Earth Syst. Sci., 20, 2175–2193, https://doi.org/10.5194/nhess-20-2175-2020, 2020.

Huh, K. I., Mark, B. G., Ahn, Y., and Hopkinson, C.: Volume change of tropical peruvian glaciers from multi-temporal digital elevation models and volume–surface area scaling, Geogr. Ann. Ser. Phys. Geogr., 99, 222–239, https://doi.org/10.1080/04353676.2017.1313095, 2017.

Huss, M. and Farinotti, D.: Distributed ice thickness and volume of all glaciers around the globe, J. Geophys. Res. Earth Surf.,
525   117, https://doi.org/10.1029/2012JF002523, 2012.

Huss, M. and Hock, R.: Global-scale hydrological response to future glacier mass loss, Nat. Clim. Change, 8, 135–140, https://doi.org/10.1038/s41558-017-0049-x, 2018.

Hutter, K.: The Effect of Longitudinal Strain on the Shear Stress of an Ice Sheet: In Defence of Using Stretched Coordinates, J. Glaciol., 27, 39–56, https://doi.org/10.3189/S0022143000011217, 1981.

530   Kaser, G.: Glacier-climate interaction at low latitudes, J. Glaciol., 47, 195–204, https://doi.org/10.3189/172756501781832296, 2001.

Kaser, G. and Georges, C.: On the mass balance of low latitude glaciers with particular consideration of the Peruvian Cordillera Blanca, Geogr. Ann. Ser. -Phys. Geogr., 81A, 643–651, 1999.

Kaser, G. and Osmaston, H.: Tropical Glaciers, The Press Syndicate of the University of Cambridge, New York, 2002.

535   Kaser, G., Juen, I., Georges, C., Gómez, J., and Tamayo, W.: The impact of glaciers on the runoff and the reconstruction of mass balance history from hydrological data in the tropical Cordillera Blanca, Perú, J. Hydrol., 282, 130–144, https://doi.org/10.1016/S0022-1694(03)00259-2, 2003.

King, O., Dehecq, A., Quincey, D., and Carrivick, J.: Contrasting geometric and dynamic evolution of lake and land-terminating glaciers in the central Himalaya, Glob. Planet. Change, 167, 46–60, https://doi.org/10.1016/j.gloplacha.2018.05.006, 2018.

540   King, O., Bhattacharya, A., Bhambri, R., and Bolch, T.: Glacial lakes exacerbate Himalayan glacier mass loss, Sci. Rep., 9, 18145, https://doi.org/10.1038/s41598-019-53733-x, 2019.

Kodama, Y.: Large-Scale Common Features of Subtropical Precipitation Zones (the Baiu Frontal Zone, the SPCZ, and the SACZ) Part I: Characteristics of Subtropical Frontal Zones, J. Meteorol. Soc. Jpn. Ser II, 70, 813–836, https://doi.org/10.2151/jmsj1965.70.4_813, 1992.

545   Mark, B. G.: Tracing tropical Andean glaciers over space and time: Some lessons and transdisciplinary implications, Glob. Planet. Change, 60, 101–114, https://doi.org/kaser, 2008.

Mark, B. G. and Seltzer, G. O.: Tropical glacier meltwater contribution to stream discharge: a case study in the Cordillera Blanca, Peru, J. Glaciol., 49, 271–281, https://doi.org/10.3189/172756503781830746, 2003.

Mark, B. G. and Seltzer, G. O.: Evaluation of recent glacier recession in the Cordillera Blanca, Peru (AD 1962–1999): spatial
550   distribution of mass loss and climatic forcing, Quat. Sci. Rev., 24, 2265–2280, https://doi.org/10.1016/j.quascirev.2005.01.003, 2005.

Mark, B. G., French, A., Baraer, M., Carey, M., Bury, J., Young, K. R., Polk, M. H., Wigmore, O., Lagos, P., Crumley, R., McKenzie, J. M., and Lautz, L.: Glacier loss and hydro-social risks in the Peruvian Andes, Glob. Planet. Change, 159, 61–76, https://doi.org/10.1016/j.gloplacha.2017.10.003, 2017.

555 Mark, B. G., Stansell, N. D., Shutkin, T., and Schoessow, F.: Glaciation and the Environments of the Cordillera Blanca, in: Geoenvironmental Changes in the Cordillera Blanca, Peru, edited by: Vilímek, V., Mark, B., and Emmer, A., Springer International Publishing, Cham, 95–115, https://doi.org/10.1007/978-3-031-58245-5_6, 2024.

Marzeion, B., Jarosch, A. H., and Hofer, M.: Past and future sea-level change from the surface mass balance of glaciers, The Cryosphere, 6, 1295–1322, https://doi-org.proxy.lib.ohio-state.edu/10.5194/tc-6-1295-2012, 2012.

560 Maussion, F., Gurgiser, W., Großhauser, M., Kaser, G., and Marzeion, B.: ENSO influence on surface energy and mass balance at Shallap Glacier, Cordillera Blanca, Peru, The Cryosphere, 9, 1663–1683, https://doi.org/10.5194/tc-9-1663-2015, 2015.

Maussion, F., Butenko, A., Champollion, N., Dusch, M., Eis, J., Fourteau, K., Gregor, P., Jarosch, A. H., Landmann, J., Oesterle, F., Recinos, B., Rothenpieler, T., Vlug, A., Wild, C. T., and Marzeion, B.: The Open Global Glacier Model (OGGM) v1.1, Geosci. Model Dev., 12, 909–931, https://doi.org/10.5194/gmd-12-909-2019, 2019.

565 Millan, R., Mouginot, J., Rabatel, A., and Morlighem, M.: Ice velocity and thickness of the world's glaciers, Nat. Geosci., 15, 124–129, https://doi.org/10.1038/s41561-021-00885-z, 2022.

Muñoz, R., Huggel, C., Frey, H., Cochachin, A., and Haeberli, W.: Glacial lake depth and volume estimation based on a large bathymetric dataset from the Cordillera Blanca, Peru, Earth Surf. Process. Landf., 45, 1510–1527, https://doi.org/10.1002/esp.4826, 2020.

570 New, M., Lister, D., Hulme, M., and Makin, I.: A high-resolution data set of surface climate over global land areas, Clim. Res., 21, 1–25, https://doi.org/10.3354/cr021001, 2002.

Oerlemans, J. and Nick, F. M.: A minimal model of a tidewater glacier, Ann. Glaciol., 42, 1–6, https://doi.org/10.3189/172756405781813023, 2005.

Ohmura, A.: Physical Basis for the Temperature-Based Melt-Index Method, J. Appl. Meteorol. Climatol., 40, 753–761, 575 https://doi.org/10.1175/1520-0450(2001)040<0753:PBFTTB>2.0.CO;2, 2001.

Pellicciotti, F., Brock, B., Strasser, U., Burlando, P., Funk, M., and Corripio, J.: An enhanced temperature-index glacier melt model including the shortwave radiation balance: development and testing for Haut Glacier d'Arolla, Switzerland, J. Glaciol., 51, 573–587, https://doi.org/10.3189/172756505781829124, 2005.

Pelto, B. M., Maussion, F., Menounos, B., Radić, V., and Zeuner, M.: Bias-corrected estimates of glacier thickness in the 580 Columbia River Basin, Canada, J. Glaciol., 1–13, https://doi.org/10.1017/jog.2020.75, 2020.

Rabatel, A., Francou, B., Soruco, A., Gomez, J., Cáceres, B., Ceballos, J. L., Basantes, R., Vuille, M., Sicart, J.-E., Huggel, C., Scheel, M., Lejeune, Y., Arnaud, Y., Collet, M., Condom, T., Consoli, G., Favier, V., Jomelli, V., Galarraga, R., Ginot, P., Maisincho, L., Mendoza, J., Ménégoz, M., Ramirez, E., Ribstein, P., Suarez, W., Villacis, M., and Wagnon, P.: Current state of glaciers in the tropical Andes: a multi-century perspective on glacier evolution and climate change, The Cryosphere, 7, 81–102, 585 https://doi.org/10.5194/tc-7-81-2013, 2013.

RGI Consortium: Randolph Glacier Inventory 6.0, https://doi.org/10.7265/N5-RGI-60, 2017.

Rodbell, D. T., Seltzer, G. O., Mark, B. G., Smith, J. A., and Abbott, M. B.: Clastic sediment flux to tropical Andean lakes: records of glaciation and soil erosion, Quat. Sci. Rev., 27, 1612–1626, https://doi.org/10.1016/j.quascirev.2008.06.004, 2008.

Sagredo, E. A. and Lowell, T. V.: Climatology of Andean glaciers: A framework to understand glacier response to climate 590 change, Glob. Planet. Change, 86–87, 101–109, https://doi.org/10.1016/j.gloplacha.2012.02.010, 2012.

Sato, Y., Fujita, K., Inoue, H., Sakai, A., and Karma: Land- to lake-terminating transition triggers dynamic thinning of a Bhutanese glacier, The Cryosphere, 16, 2643–2654, https://doi.org/10.5194/tc-16-2643-2022, 2022.

Schauwecker, S., Rohrer, M., Acuña, D., Cochachin, A., Dávila, L., Frey, H., Giráldez, C., Gómez, J., Huggel, C., Jacques-Coper, M., Loarte, E., Salzmann, N., and Vuille, M.: Climate trends and glacier retreat in the Cordillera Blanca, Peru, revisited, Glob. Planet. Change, 119, 85–97, https://doi.org/10.1016/j.gloplacha.2014.05.005, 2014.

Seehaus, T., Malz, P., Sommer, C., Lippl, S., Cochachin, A., and Braun, M.: Changes of the tropical glaciers throughout Peru between 2000 and 2016 - Mass balance and area fluctuations, Cryosphere, 13, 2537–2556, https://doi.org/10.5194/tc-13-2537-2019, 2019.

Shugar, D. H., Burr, A., Haritashya, U. K., Kargel, J. S., Watson, C. S., Kennedy, M. C., Bevington, A. R., Betts, R. A., Harrison, S., and Strattman, K.: Rapid worldwide growth of glacial lakes since 1990, Nat. Clim. Change, 1–7, https://doi.org/10.1038/s41558-020-0855-4, 2020.

Sicart, J. E., Wagnon, P., and Ribstein, P.: Atmospheric controls of the heat balance of Zongo Glacier (16 degrees S, Bolivia), J. Geophys. Res.-Atmospheres, 110, 2005.

Sicart, J. E., Hock, R., and Six, D.: Glacier melt, air temperature, and energy balance in different climates: The Bolivian Tropics, the French Alps, and northern Sweden, J. Geophys. Res. Atmospheres, 113, https://doi.org/10.1029/2008JD010406, 2008.

Stansell, N. D., Mark, B. G., Licciardi, J. M., Rodbell, D. T., Fairman, J. G., Schoessow, F. S., Shutkin, T. Y., and Sorensen, M.: Energy mass balance and flow modeling of early Holocene glaciers in the Queshque valley, Cordillera Blanca, Peru, Quat. Sci. Rev., 281, 107414, https://doi.org/10.1016/j.quascirev.2022.107414, 2022.

Stansell, N. D., Abbott, M. B., Diaz, M. B., Licciardi, J. M., Mark, B. G., Polissar, P. J., Rodbell, D. T., and Shutkin, T. Y.: Pre-industrial Holocene glacier variability in the tropical Andes as context for anthropogenically driven ice retreat, Glob. Planet. Change, 229, 104242, https://doi.org/10.1016/j.gloplacha.2023.104242, 2023.

Sutherland, J. L., Carrivick, J. L., Gandy, N., Shulmeister, J., Quincey, D. J., and Cornford, S. L.: Proglacial Lakes Control Glacier Geometry and Behavior During Recession, Geophys. Res. Lett., 47, e2020GL088865, https://doi.org/10.1029/2020GL088865, 2020.

Tangborn, W. V., Fountain, A. G., and Sikonia, W. G.: Effect of Area Distribution with Altitude on Glacier Mass Balance – A Comparison of North and South Klawatti Glaciers, Washington State, U.S.A., Ann. Glaciol., 14, 278–282, https://doi.org/10.3189/S0260305500008752, 1990.

Thompson, L. G., Mosley-Thompson, E., Davis, M. E., and Brecher, H. H.: Tropical glaciers, recorders and indicators of climate change, are disappearing globally, Ann. Glaciol., 52, 23–34, https://doi.org/10.3189/172756411799096231, 2011.

Vuille, M.: Rapid decline of snow and ice in the tropical Andes – Impacts, uncertainties and challenges ahead, Earth-Sci. Rev., 176, 195–213, https://doi.org/10.1016/j.earscirev.2017.09.019, 2018.

Vuille, M., Francou, B., Wagnon, P., Juen, I., Kaser, G., Mark, B. G., and Bradley, R. S.: Climate change and tropical Andean glaciers: Past, present and future, Earth-Sci. Rev., 89, 79–96, https://doi.org/10.1016/j.earscirev.2008.04.002, 2008a.

Vuille, M., Kaser, G., and Juen, I.: Glacier mass balance variability in the Cordillera Blanca, Peru and its relationship with climate and the large-scale circulation, Glob. Planet. Change, 62, 14–28, https://doi.org/10.1016/j.gloplacha.2007.11.003, 2008b.

Wagnon, P., Ribstein, P., Kaser, G., and Berton, P.: Energy balance and runoff seasonality of a Bolivian glacier, Glob. Planet. Change, 22, 49–58, https://doi.org/10.1016/S0921-8181(99)00025-9, 1999.

Wood, J. L., Harrison, S., Wilson, R., Emmer, A., Yarleque, C., Glasser, N. F., Torres, J. C., Caballero, A., Araujo, J., Bennett, G. L., Diaz-Moreno, A., Garay, D., Jara, H., Poma, C., Reynolds, J. M., Riveros, C. A., Romero, E., Shannon, S., Tinoco, T., Turpo, E., and Villafane, H.: Contemporary glacial lakes in the Peruvian Andes, Glob. Planet. Change, 204, 103574, https://doi.org/10.1016/j.gloplacha.2021.103574, 2021.

Zhou, J. and Lau, K.-M.: Does a Monsoon Climate Exist over South America?, J. Clim., 11, 1020–1040, https://doi.org/10.1175/1520-0442(1998)011<1020:DAMCEO>2.0.CO;2, 1998.